Solar Energy Materials & Solar Cells 240 (2022) 111731

Contents lists available at ScienceDirect

Solar Energy Materials and Solar Cells

journal homepage: www.elsevier.com/locate/solmat

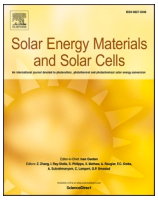

Interdigitated back-contacted crystalline silicon solar cells fully manufactured with atomic layer deposited selective contacts

Gerard Masmitjà *, Eloi Ros, Rosa Almache-Hernández, Benjamín Pusay, Isidro Martín, Cristóbal Voz, Edgardo Saucedo, Joaquim Puigdollers, Pablo Ortega

Electronic Engineering Department, Universitat Politècnica de Catalunya, Jordi Girona 1 – 3, 08034, Barcelona, Spain

ARTICLE INFO

Keywords:
Atomic layer deposition
Interdigitated back-contacted solar cells
Selective contacts
Surface passivation
Contact resistivity
Vanadium oxide

ABSTRACT

The interdigitated back-contacted (IBC) solar cell concept has been extensively studied for single-junction cells and more recently as a good choice for three-terminal tandem devices. In this work, carrier-selective contacts based on transition metal oxides deposited by atomic layer deposition (ALD) technique are applied to IBC c-Si(n) devices. In the first part of the study, we develop a hole-selective contact based on thin ALD vanadium oxide (V_2O_5) layers without using an amorphous silicon interlayer. The ALD process has been optimised, i.e. number of ALD cycles and deposition temperature, as a trade-off between surface passivation and contact resistivity. Noticeable surface passivation with recombination current densities around 100 fA/cm^2, as well as reasonable contact resistivity values below 250 mΩcm^2 are reached using 200 ALD V_2O_5 cycles deposited at a deposition temperature of 125 °C (~10 nm layer thickness). The optimised ALD V_2O_5-based contact is combined with both an ALD TiO_2-based electron-selective contact and an excellent surface passivation in non-contacted regions provided by ALD Al_2O_3 films, to form a fully ALD IBC c-Si(n) solar cell scheme. Fabricated devices yield photovoltaic efficiencies and pseudo efficiencies, i.e. calculated without series resistance losses, of 18.6% and 21.1% respectively (3 cm × 3 cm device area). These results reveal the potential of the ALD technique to deposit transition metal oxide (TMO) films as selective contacts on high efficiency devices, paving the way of using low thermal-budget, low cost and highly scalable processes for a highly demanding IBC solar cell architecture in the photovoltaic industry.

1. Introduction

The photovoltaic market is dominated by crystalline silicon (c-Si) solar cells [1]. The charge-carrier selectivity at the contacts of these devices is mainly achieved by phosphorous and boron diffusion species inside the c-Si substrate, the so-called pn junction. Another way to obtain contact selectivity, i.e. a good balance between resistance and passivated contact properties, is the use of a heterojunction structure (SHJ), in which doped hydrogenated amorphous silicon (a-Si:H) films act as selective contacts. In fact, the highest energy conversion efficiency is achieved with SHJ-based contacts with an efficiency of 26.7% [2]. Moreover, this record cell efficiency is accomplished by using an interdigitated back-contacted (IBC) scheme. In IBC cells both contacts, the electron (ETL) and the hole (HTL) transport layers, are placed on the back of the device. Thus, the front surface is free from metal pads and a-Si:H films, which cause losses due to shadowing [3] and parasitic optical absorption [4], respectively. By doing so, light absorption in the c-Si substrate increases and consequently, the cell photocurrent and conversion efficiency are enhanced.

Recently, IBC solar cells have been proposed as the bottom cell of a three-terminal tandem device [5]. The main challenge of a monolithic two-terminal tandem structure is the current matching between the lower and upper cell. However, with an IBC bottom cell, a three-terminal tandem architecture is feasible, where the two generated photocurrents can be extracted separately, maximising the efficiency of both cells [6]. This concept broadens the interest of IBC cells, not only for their initial use, which was focused on concentrating solar applications, but also for emerging tandem architectures [7].

In laboratory and industrial solar cells, high conversion efficiency is usually achieved using pn-based or a-Si:H junctions. However, interesting approaches have been studied in the past to find alternatives that avoid the use of high temperature steps or flammable gaseous

* Corresponding author.
E-mail address: gerard.masmitja@upc.edu (G. Masmitjà).

https://doi.org/10.1016/j.solmat.2022.111731
Received 30 November 2021; Received in revised form 25 March 2022; Accepted 29 March 2022
Available online 2 April 2022

precursors, involved in these technologies. In this way, transition metal oxides (TMOs) [8], such as vanadium (V_2O_x) [9], molybdenum (MoO_x) [10], titanium (TiO_x) [11] or magnesium (MgO_x) [12] oxides, are promising candidates. TMOs have a wide range of work function values, which allow either an alignment of energy levels between the absorber and the metal electrode or the introduction of a highly inverted/accumulated region under the silicon-contact interface, improving in both cases the contact selectivity [13]. In addition, their wide bandgap (>3 eV) makes them transparent [9], minimising parasitic optical absorption, as well as suitable antireflection or back-reflector contact materials. Benefits of TMOs applied to c-Si solar cells and in particular to an IBC structure are systemically studied and evaluated in the literature, see for instance Refs. [14–16]. Table 1 summarises the main reported contributions elsewhere using an IBC cell structure and TMO-based contacts highlighting their deposition technology.

TMOs described in the literature are usually deposited by thermal evaporation technique, which does not provide a simple scalable route for the photovoltaic industry. With this issue in mind, the atomic layer deposition (ALD) technique has sparked interest in TMO deposition [17–21], not only because of the excellent control of film growth and uniformity in large-area devices, but also because of the possibility of reasonable film deposition rates. Although the standard laboratory ALD process exhibits a slow deposition rate, it has already been reported that the spatial ALD technique, which is an ALD system with its reactors spatially separated [22], is capable of depositing alumina (Al_2O_3) films at rates as high as 1.2 nm/s providing at the same time excellent surface passivation [23]. Another promising example is the use of spatial ALD to deposit MoO_x films as HTL at rates of 5.4 nm/min [17].

Finally, the ALD V_2O_5 films have recently been published as a hole-selective contact in c-Si solar cells [18]. Although careful characterisations have been performed in the aforementioned work, such as passivation properties on p- and n-type c-Si substrates, the contact resistivity is only reported for p-type wafers. Moreover, the V_2O_5-based contact implemented in the solar cell is performed with the help of an intrinsic a-Si:H interlayer. In a recent work, we also reported the use of ALD V_2O_5 films for c-Si(n) solar cells [24], in which the ALD V_2O_5 film was placed on the front side together with an indium tin oxide (ITO) layer. Nonetheless, a conventional vertical cell structure and an n-doped a-Si:H stack as the electron-selective contact, were used for these devices.

This work focuses on applying the ALD V_2O_5 films, without an a-Si:H interlayer, as hole-selective contacts on n-type c-Si solar cells using an IBC architecture. Furthermore, the IBC cell is fully implemented with ALD-based films, which means that both the hole-selective and the electron-selective contacts are based on ALD V_2O_5 and TiO_x films, respectively. In addition, the front and rear non-contacted surfaces are passivated with Al_2O_3 films also deposited by ALD. The V_2O_5 characterisation and its electrical/passivation behaviour as HTL is extensively reported in the next sections, exhibiting good surface passivation and relatively low contact resistivity. The ALD TiO_x characterisation was reported in our previous studies, see Ref. [20]. The main goal of this work is to demonstrate that fully ALD IBC solar cells could be developed circumventing the use of a-Si:H interlayers and reaching relevant efficiencies in 3 × 3 cm^2 devices. These results pave the way for low thermal-budget, low cost and highly scalable ALD processes in combination with a highly demanding IBC solar cell architecture in the photovoltaic fabrication chain.

Table 1
Summary of the main reported IBC solar cells using TMOs as selective contacts.

Ref.	Selective contact strategy (deposition method)		Efficiency (%)	Year
	HTL	ETL		
[25]	MoO_x (thermal evap.)	LiF_x (thermal evap.)	15.4	2016
[26]	V_2O_x (thermal evap.)	Cs_2CO_3 (thermal evap.)	16.6	2016
[27]	V_2O_x/Au/V_2O_x (thermal evap.)	LiF_x (thermal evap.)	19.0	2017
[20]	V_2O_x (thermal evap.)	Al_2O_x/TiO_x (ALD)	19.1	2018
[28]	a-Si:H(i)/MoO_x (thermal evap.)	a-Si:H(i)/MgF_x (thermal evap.)	22.2	2018
[29]	PEDOT:PSS (spin-coating)	MgO_x (thermal evap.)	16.3	2018
[30]	a-Si:H(i)/MoO_x (hot-wire sublimation)	a-Si:H(i)/SiO_x/TiO_x (spin-coating)	20.2	2019
[31]	a-Si:H(i)/MoO_x (thermal evap.)	a-Si:H(i)/LiF_x (thermal evap.)	20.3	2020
[32]	a-Si:H(i)/MoO_x (thermal evap.)	a-SI:H(i)/MgF_x (thermal evap.)	22.1	2020
This work	**V_2O_5 (ALD)**	**Al_2O_x/TiO_x (ALD)**	**18.6**	–

2. Experimental methods

2.1. ALD characterisation and film morphology

An ALD process and material characterisation of vanadium oxide layers were studied with FZ < 100> c-Si(n) substrates with thickness and resistivity of 280 μm and ~2 Ωcm, respectively. After a HF (2%) dip for 30 s, the samples were introduced to the ALD equipment to deposit the corresponding V_2O_5 film.

Vanadium oxide films were deposited by a thermal ALD system (Savannah S200, Cambridge Nanotech) with tetrakis (ethylmethylamino)-vanadium(IV) (VTIP) and deionised water (DI-H_2O) as the vanadium precursor and oxidant species, respectively. The VTIP and water cylinders were set to 58 °C and room temperature, respectively. The influence of the main parameters involved in the ALD process, such as purges, precursor and oxidant pulse times, were evaluated by monitoring the film growth rate to ensure a self-limiting surface reacting regime. Moreover, the ALD process characterisation was studied for a temperature range from 80 °C to 200 °C.

The V_2O_5 film structure and morphology were studied by X-ray photoelectron spectroscopy (XPS), using for the measurements a non-monochromatic Al-Kα source (1486.6 eV) at 3 × 10^{-9} mbar (SPECS, hemispherical energy analyser PHOIBOS 150). High angle annular dark field (HAADF) scanning TEM images, in combination with energy dispersive X-ray spectroscopy (EDX) chemical composition analysis were executed by using a Cs-corrected FEI Titan (60–300 kV) transmission electron microscope. The FEI Titan was equipped with a high brightness Schottky emitter source (X-FEG gun), a monochromator and a Gatan 2k × 2 k CCD camera. The cross-section lamellas were prepared from contact test samples, using a focused ion beam (FIB) lift-out technique. The samples were subjected to an oxygen plasma cleaning process before introducing them into the FEI Titan equipment.

2.2. Passivation test samples

The passivation properties of ALD V_2O_5 films were studied in symmetrical samples using the same c-Si(n) substrates. A cleaning process with a 30 s dip in diluted HF (2%) was performed just before the introduction of the sample in the ALD equipment. In some test samples, c-Si(n) substrates were replaced using p-type counterparts with similar characteristics and same sample preparation.

The impact of the metal capping in the V_2O_5-based contact behaviour was assessed in another set of samples using the same c-Si(n) substrates. In this case, the V_2O_5 film was deposited only in the front side and covered with a semi-transparent Ni film using an asymmetrical structure as follows (see Ref. [33] for details): first, after a RCA1/RCA2 and HF dip cleaning sequence [34], the samples were covered with a 50 nm thick ALD Al_2O_3 layer on both sides deposited at 200 °C. Trimethylaluminium (TMA) and DI-H_2O were used as the Al precursor and oxidant species, respectively. Next, the rear side was covered with a 25 nm thick silicon carbide layer (a-SiC). This close to stoichiometric a-SiC_x film (x~1) was deposited by a plasma-enhanced chemical vapour deposition (PECVD)

process (13.56 MHz, from Electtrorava S.p.A) at 300 °C, using methane and silane as precursor gases. The a-SiC layer provides an Al_2O_3 film protection for subsequent chemical processes. At this point, the samples underwent an annealing treatment at 400 °C for 10 min in forming gas ambient to activate the surface passivation [35]. After etching the front Al_2O_3 layer with a HF (2%) dip, the corresponding ALD V_2O_5 film was deposited (200 ALD cycles at 125 °C). Afterwards, the V_2O_5 film was covered with a thermally evaporated nickel film with a thickness of ~5 nm. The semi-transparent Ni film (~5 nm) allows reliable QSS-PC measurements in order to determine the influence of the metallic film on surface passivation.

Surface passivation was assessed by effective lifetime measurements by means of the quasi-steady-state photoconductance (QSS-PC) technique [36] using the WCT-120 instrument (Sinton Consulting).

2.3. Contact test samples

The contact properties of ALD V_2O_5 films were also studied using the aforementioned c-Si(n) substrates. A cleaning process with a 30 s dip in diluted HF (2%) was conducted just before the introduction of the sample in the ALD equipment. In some test samples, c-Si(n) substrates were replaced using p-type counterparts with similar characteristics.

Contact characteristics were obtained using the transfer length method (TLM) [37,38]. Just after the ALD V_2O_5 film deposition, TLM patterned metal-pads were evaporated above the V_2O_5 film using a metallic shadow mask. Metallisation consists of a Ni/Al stack with a thickness of ~10/300 nm, respectively. The stack was thermally evaporated from pure source materials >99.95% using an SQC-310 deposition controller (Sigma instruments).

The electrical contact behaviour on c-Si(p) samples was assessed by fitting the dependence of the measured resistance of vertical dot-like structures as a function of the dot diameter, using the spreading resistance model [39]. In this case, just after the ALD V_2O_5 film deposition on both sides of the sample, dot-like metal contacts (Ni/Al) were evaporated above the V_2O_5 film using a metallic shadow mask (front side). Then, the same metal stack was evaporated on the back side, above the V_2O_5 film, resulting in a fully contacted surface.

Electrical measurements were performed using a four-contact probe configuration by means of a current voltage (*I–V*) tracer (Keithley 3601B) at room temperature.

2.4. Solar cells

Finally, IBC solar cells of 3 × 3 cm^2 active area were fabricated using the same c-Si(n) substrates. The fabrication process starts with a front side random pyramid texturing by alkaline etching, using a tetramethylammonium hydroxide (TMAH) based solution. Then, the wafer was cleaned following a RCA1/2 sequence and a 50 nm thick Al_2O_3 layer was deposited on both sides by ALD at 200 °C, using TMA and DI-H_2O species. To activate the surface passivation provided by the alumina film, a 10 min annealing step was performed at 400 °C. Then a 25 nm thick a-SiC film was deposited on both sides in a similar way as explained before in the test samples (see section 2.2).

After a strip-like patterning on the c-Si back surface by tetrafluoromethane (CF_4) plasma dry etching and a diluted RCA1/2 sequence, removing the a-SiC and Al_2O_3 films, respectively, the ETL based on an Al_2O_x/TiO_x stack was deposited by ALD at 100 °C. This TiO_2-based contact scheme has been described in detail in one previous work of our group [20]. Afterwards, a Mg/Al stack was thermally evaporated resulting in 25 nm and 3 μm thick layers, respectively. Subsequently, the interdigitated electrodes were patterned by standard photolithography and wet etching. The whole back surface was covered with a structural photosensitive polyimide layer and the HTL strip-like regions were defined by photolithography. Thereafter, the a-SiC and alumina films were removed by a CF_4 dry etching and a subsequent HF dip. Finally, the ALD V_2O_5 film was deposited and covered by a nickel capping layer (~10 nm) and a 2 μm thick Al film. The whole metal stack was thermally evaporated using a shadow mask to avoid an additional photolithographic step, simplifying the fabrication process.

Photovoltaic parameters and illuminated *I–V* curves were measured under standard test conditions (1 kW/m^2 AM1.5G solar spectrum at a temperature of 25 °C) using an ORIEL 94021A (Newport) solar simulator. Light irradiance was properly calibrated by means of a pyranometer. External-quantum-efficiency (EQE) curves were measured using a commercial instrument (QEX10, PV measurements) with a white light bias of 0.1 Suns and a beam spot of 2 × 2 cm^2 centred within the active device area.

3. Results and discussion

3.1. ALD characterisation

Test samples of crystalline silicon covered with 600 ALD cycles of V_2O_5 were made in order to characterise the film growth and optimise the ALD deposition parameters. The inset of Fig. 1 shows the growth per cycle (GPC) with respect to H_2O and VTIP pulse durations with a process temperature of 125 °C. In all cases, the VTIP and water purge times were of 5 s. Two seconds H_2O pulses were enough to achieve a GPC saturation condition, but a much longer pulse was required for the VTIP precursor. Thus, a 5 s VTIP pulse was chosen as a trade-off between the process duration and quasi self-saturation regime. Notice, that a GPC of 0.6 Å/cycle is achieved, which is comparable to other reported studies using the same vanadium precursor [40,41].

Then, the growth characteristics of the ALD V_2O_5 film were investigated in a temperature range from 80 to 200 °C. The GPC is shown in Fig. 1, where the self-saturation ALD regime occurs in a wide temperature window between 80 and 150 °C, with a growth rate of ~0.6 Å/cycle. For higher temperatures, the growth rate quickly increases pointing out a chemical vapour deposition (CVD) regime.

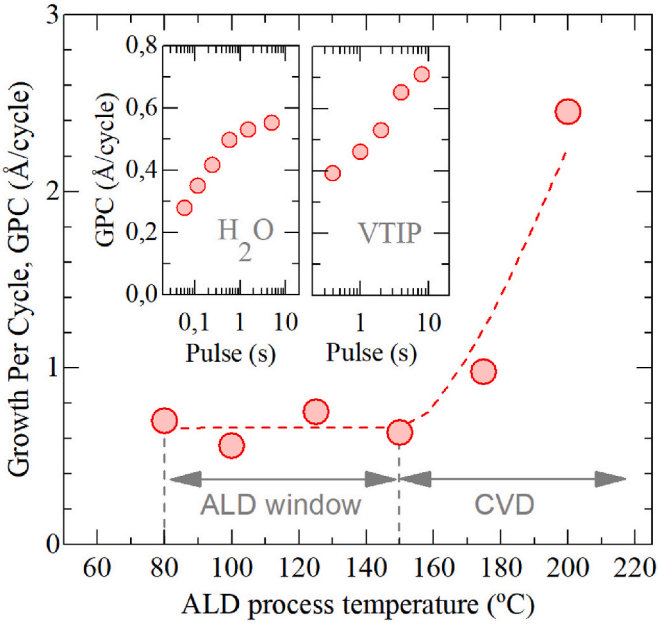

Fig. 1. Growth per cycle (GPC) rate as a function of the deposition temperature, using H_2O and VTIP pulses of 2 and 5 s, respectively. In all cases purge times between precursor and water pulses were of 5 s (using N_2 flow). The insets show the GPC as a function of the H_2O pulse duration with a fixed VTIP pulse of 2 s (left), and the VTIP pulse duration with a fixed H_2O pulse of 2 s (right). In both cases using a deposition temperature of 125 °C.

3.2. Passivation and electrical properties

Once the V_2O_5 ALD process was optimised, lifetime and transmission line method (TLM) measurements were carried out to determine the recombination current density (J_{0c}) and the contact resistivity (ρ_c), respectively. Low values of J_{0c} and ρ_c are mandatory to obtain good selective contact behaviour, and thus to obtain high efficiency c-Si solar cells.

The inset in Fig. 2a shows the measured lifetime on symmetrical samples covered with 200 ALD cycles of V_2O_5 for different deposition temperatures from 100 to 150 °C. In all cases, the optimum ALD process condition described in section 3.1 was used, i.e. 2/5/5/5 s of H_2O/purge/VTIP/purge, respectively. J_{0c} values were extracted from effective lifetime (τ_{eff}) measurements [36]. A general trend can be observed in Fig. 2a, pointing out that a better passivation is achieved for lower ALD process temperatures. An implied open circuit voltage (iV_{oc}) value of 655 mV and a J_{0c} value of 80 fA/cm^2 were achieved at 100 °C. For higher process temperatures, i.e. 125 °C and 150 °C, the J_{0c} parameter increases to 100 fA/cm^2 and 150 fA/cm^2 respectively. In any case, ALD V_2O_5 films achieve a better passivation behaviour compared to thermally evaporated V_2O_5 films, where J_{0c} values of 175 fA/cm^2 were obtained [33].

The impact of the V_2O_5 film thickness, ranging from 50 to 300 ALD cycles, on the passivation behaviour is shown in Fig. 2b. In all cases, the process temperature was fixed at 125 °C. The film thickness has a lower impact on the passivation properties, showing only slight variations, with J_{0c} values of around 100 fA/cm^2. This trend is not observed by other researchers; see for instance Ref. [18], where the J_{0c} values decrease for thicker films, yielding J_{0c} values from 95 to 40 fA/cm^2 for VO_x thickness from 4 to 9 nm, respectively.

Finally, the contact passivation provided by ALD V_2O_5 films was also studied for p-type c-Si substrates, obtaining similar results, with a J_{0c} value of 100 fA/cm^2 (see Fig. 2b).

Additionally, the effect of an alumina interlayer between the c-Si and the V_2O_5 layer was explored. Our previous reports indicate a passivation improvement by using an ultrathin ALD Al_2O_3 film between the c-Si surface and the ALD TiO_2 layer [20]. However, applied to V_2O_5 films, 6 ALD cycles of an Al_2O_3 interlayer considerably increased the J_{0c} value, i.e. worse contact passivation with a value of ~200 fA/cm^2. Therefore, the alumina interlayer is not convenient for passivating V_2O_5 contacts. This result agrees with other studies in which the alumina film was applied to contacts based on MoO_x layers showing a modest impact on selective properties [42].

TLM measurements were performed on c-Si(n) samples covered with a 200 ALD cycles V_2O_5 film and contacted with a Ni/Al stack. It is reported that the metal contact can affect the electrical properties on thin TMO films [43]. Additionally, in a previous result reported in Ref. [33] we concluded that a high-work function metal like Ni is preferred to contact thermally evaporated V_2O_5 layers in comparison to low-work function metals like Al. More recently, other researchers have also used Ni as capping material for high-work function MoO_x films, resulting in a clear reduction of contact resistivity [17]. Thus, it is expected that Ni could also be a good candidate to contact the ALD V_2O_5 films. Fig. 3a shows the contact resistivity (ρ_c) as a function of the ALD process temperature. The TLM measurements confirm a minimum ρ_c value, lower than 250 mΩcm^2 using 200 cycles and an ALD process temperature of 125 °C.

The TLM measurements were also used to extract the sheet resistance parameter (R_{sh}) of the depleted/inverted region beneath the HTL contact, obtaining values between 11 and 16 kΩ/sq for all the studied temperature range. The R_{sh} parameter was also measured by means of TLM structures on a glass substrate, as can be seen in the inset of Fig. 3a showing values higher than 5 GΩ/sq attributed to the V_2O_5 layer. Consequently, the lower value obtained in the c-Si(n) substrates confirms the presence of an inverted p^+ layer on the n-type silicon surface underneath the film, reinforcing the hole-selective behaviour of the contact. It is interesting to highlight the relationship between the R_{sh} and surface passivation. The lower the R_{sh} value is the lower is also J_{0c}. This relation seems to indicate that a stronger inversion occurs inside the c-Si substrate, leading to a better passivated contact.

The impact of the V_2O_5 film thickness, i.e. number of ALD cycles, on the contact resistivity was also studied considering a process temperature of 125 °C (see Fig. 3b). Notice that the film thickness has a high influence on the ρ_c parameter. For small thicknesses, the contact quality is very poor, achieving a high ρ_c value of ~1 Ωcm^2 for 50 ALD cycles. Nevertheless, a minimum ρ_c was found for 200 ALD cycles with a value of 250 mΩcm^2, increasing again for thicker layers.

The influence of a thin ALD Al_2O_3 interlayer in the contact properties was also included in the study. Again, the presence of this film worsens the contact behaviour, obtaining a ρ_c value of 550 mΩcm^2. In addition, vertical test measurements were performed with c-Si(p) substrates following the sample preparation described in the experimental section and using 200 ALD cycles of V_2O_5 film. Although the passivation was similar independent of the substrate type, the ρ_c shows a better behaviour using c-Si(p) substrates. A contact resistivity of 100 mΩcm^2 was obtained, which is comparable to the best values reported in the literature, for a c-Si(p)/VO_x/Ag contact scheme [18]. Hence, we can conclude that a Ni-capped ALD V_2O_5 layer has a very good performance

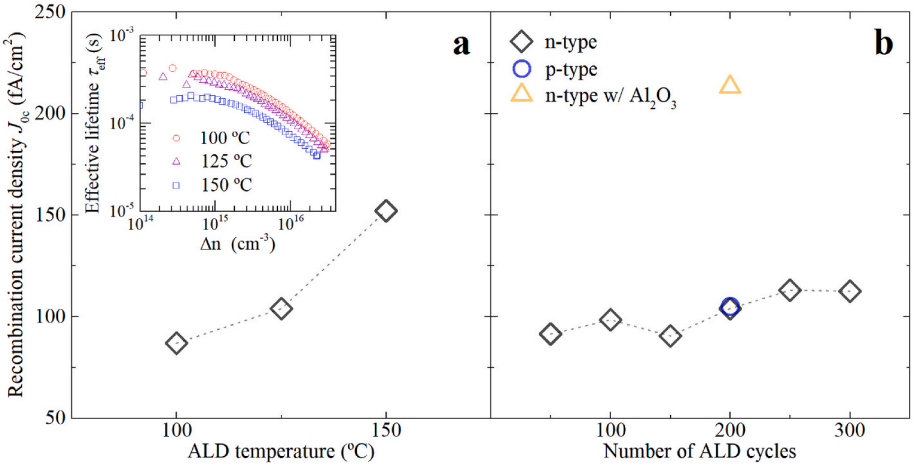

Fig. 2. Recombination current density (J_{0c}) as a function of the ALD process temperature (left) and the number of ALD cycles (right). Measured lifetime (τ_{eff}) for different ALD process temperatures are also shown (inset). For the temperature study the c-Si was covered on both side with 200 ALD cycles of V_2O_5 film. For the thickness study the ALD temperature was kept at 125 °C.

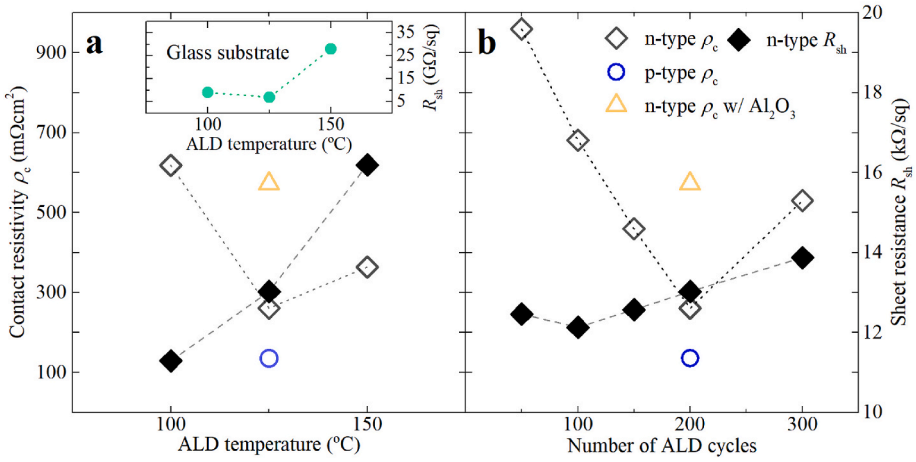

Fig. 3. Contact resistivity (empty symbols) and sheet resistance (filled symbols) as a function of the ALD process temperature (left) and the number of ALD cycles (right). R_{sh} values extracted from glass substrates are also shown in the inset. For the ALD temperature study (left), the c-Si was covered with 200 ALD cycles of a V_2O_5 film. For the number of ALD cycles study (right), the ALD temperature was kept at 125 °C (ρ_c and R_{sh} values were extracted from TLM using Ni/Al pads).

to contact c-Si substrates.

Finally, the impact of Ni metallisation on surface passivation was evaluated using a very thin Ni film (~5 nm) deposited on the V_2O_5 layer in order to mimic the final contacted structure in solar cell devices. In this case, an asymmetric scheme was used, in which the rear side was passivated with an Al_2O_3/a-SiC stack and the front side was passivated with a V_2O_5 layer as explained in the experimental section. A film of V_2O_5 consisting of 200 ALD cycles deposited at 125 °C was chosen as the best option considering the trade-off between ρ_c and J_{0c} values. The excellent passivation properties provided by ALD Al_2O_3 layers [35], i.e. effective surface recombination velocity (S_{eff}) values below 2 cm/s, allow discriminating the recombination contribution of the Al_2O_3-coated side, thus obtaining the recombination contribution of the V_2O_5-coated surface. Fig. 4a shows the measured lifetime of a both-sides passivated sample with an ALD Al_2O_3 film with its associated intrinsic lifetime (τ_{in}) [44] (upper limit), reaching an S value as low as 1.6 cm/s (J_{0c} ~5 fA/cm^2) [45]. Comparing lifetime results of asymmetric samples with and without a Ni film (see Fig. 4a), we can conclude that the metal capping does not affect the passivation quality, with J_{0c} values around 100 fA/cm^2 in either case.

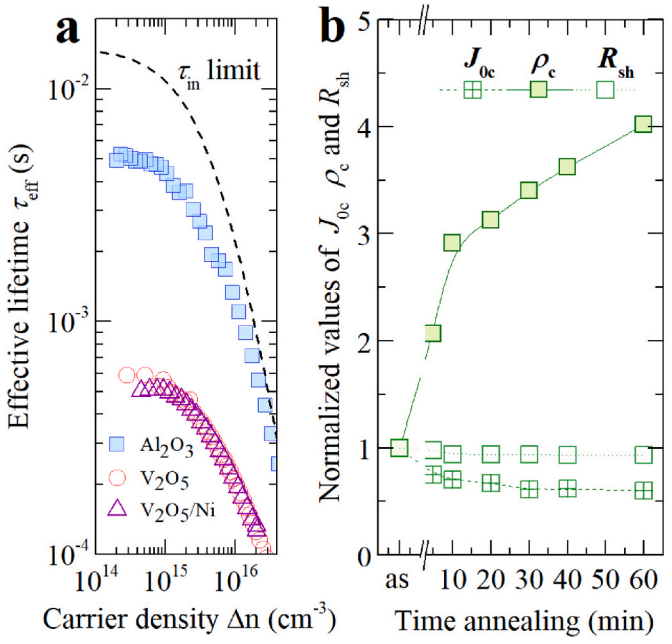

Fig. 4. Measured lifetime (τ_{eff}) for Al_2O_3/c-Si(n)/Al_2O_3, V_2O_5/c-Si(n)/Al_2O_3 and Ni/V_2O_5/c-Si(n)/Al_2O_3 samples (left). Normalised recombination current density (J_{0c}), contact resistivity (ρ_c) and sheet resistance (R_{sh}) as a function of the annealing accumulative time (right). All annealing stages were performed at 125 °C in N_2 ambient. J_{0c} values were extracted from τ_{eff} measurements and ρ_c and the R_{sh} values from TLM structures.

Fig. 4b shows the evolution of the normalised values (i.e. value$_{measured}$/value$_{initial}$) of J_{0c}, ρ_c and R_{sh} parameters for accumulative annealing times at 125 °C in N_2. Regarding surface passivation, the contact shows an improvement with the annealing time. Note that the J_{0c} value decreases by 30% after the initial 10 min annealing. However, the contact resistivity degrades strongly with the annealing time. The ρ_c value evidences a three-fold increase with an annealing of only 10 min. Therefore, the V_2O_5-based selective contact should be deposited at the last stages of the IBC fabrication process to avoid any high thermal steps which would jeopardise the good contact behaviour.

3.3. Morphological properties

Physical and morphological characterisation of the V_2O_5-based contact was analysed in order to determine the origin of the good electrical performance of the hole-selective contact. Firstly, an X-ray photoelectron spectroscopy (XPS) scan was performed on a 10 nm thick ALD V_2O_5 film deposited on a c-Si substrate. Fig. 5 shows the XPS core level spectra for the V_2O_5 film deposited at 125 °C. The V 2p core level was decomposed into a single peak centred at a binding energy of 516.9 eV, which can be attributed to the presence of V^{+5} cations [46]. This characteristic elucidates that the film has a stoichiometric V_2O_5 phase and thus, no significant O vacancy defects are present. Hence, the main conduction mechanism through the layer might be a tunnelling process and not a trap-assisted process. The higher work function of stoichiometric films causes a stronger band bending inside the c-Si substrate, allowing holes to tunnel directly from the c-Si to the contact [17]. In addition, the Si 2p core level spectra are represented, in which a secondary peak centred at a binding energy of 101.8 eV is needed for the fitting. This binding energy is attributed to the presence of Si^{+3} oxidation states related to suboxidised SiO_x films, corroborated with the O 1s core level spectra.

Further analysis of the c-Si/V_2O_5/Ni/Al stack was performed by a high angle annular dark field (HAADF) scanning TEM image in combination with an energy dispersive X-ray spectroscopy (EDX) analysis. The EDX confirms the composition of the hole-selective contact structure (see Fig. 6), which is an ~10 nm thick V_2O_5 layer and a ~7 nm thick Ni film.

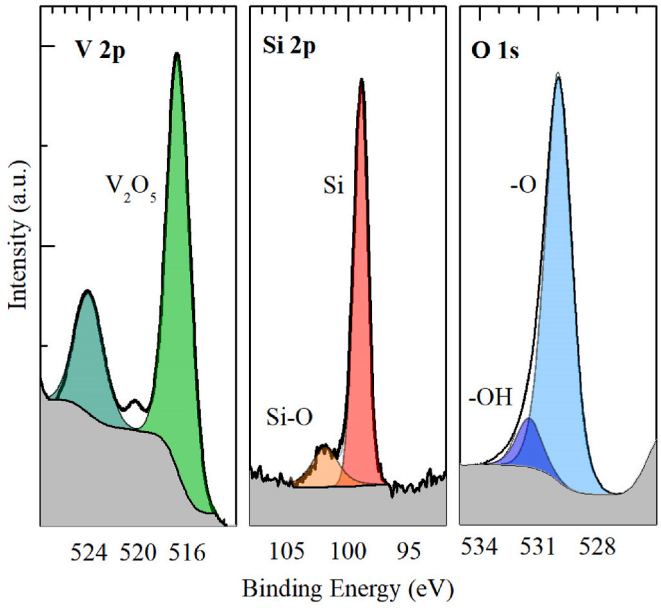

Fig. 5. X-ray photoelectron spectroscopy core-level spectra of V 2p, Si 2p and O 1s for the ALD V_2O_5 film deposited at 125 °C on c-Si(n) substrates.

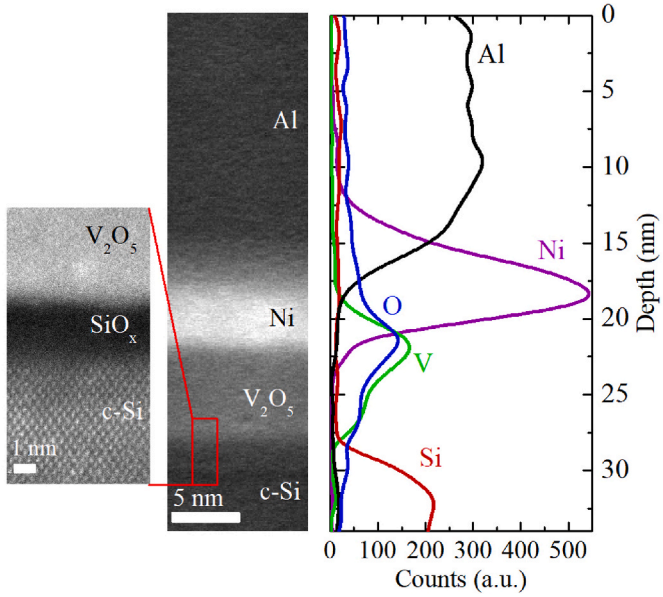

Fig. 6. Cross-sectional HR-TEM image of the c-Si/V_2O_5 interface (left) and HAADF STEM image (middle) and EDX line scan of the c-Si/V_2O_5/Ni/Al structure with the Al, Ni, V, O and Si concentrations (right).

The presence of a thin interlayer between V_2O_5 and c-Si is observed with the cross-sectional high-resolution transmission electron microscopy (HR-TEM) image, verifying the XPS analysis. The SiO_x interlayer has a thickness of about 1.6 nm. The formation of such silicon oxide layer has been previously observed in thermally evaporated TMOs [47] and also for the ALD process [17,18]. The good passivation properties of the TMOs are attributed, in part to the presence of this ultra-thin SiO_x interlayer.

3.4. IBC c-Si solar cells

The best ALD V_2O_5-based contact configuration was applied to fabricate proof-of-concept 3 × 3 cm^2 IBC c-Si(n) solar cells. Fig. 7 shows

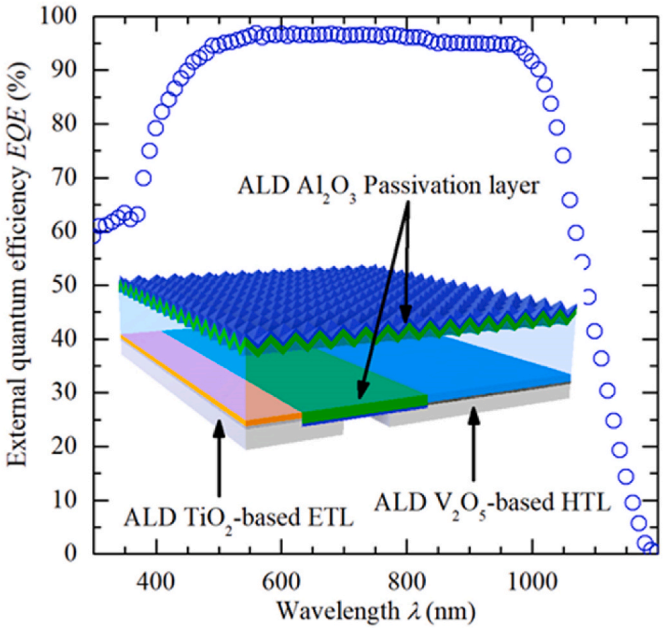

Fig. 7. EQE curve of the best fully-ALD IBC solar cell. A 3D sketch of IBC solar cell is shown in the inset. Notice that the front surface and the gap between strip-like contacts are passivated with ALD Al_2O_3 films.

a device 3D sketch highlighting that all surfaces of the silicon are covered with films deposited by the ALD technique. Specifically, a V_2O_5 film (200 ALD cycles deposited at 125 °C) for the hole-selective contact, an Al_2O_x/TiO_x stack (6/20 ALD cycles) for the electron-selective contact [20] and a thick Al_2O_3 layer (500 ALD cycles) to passivate non-contacted regions, i.e. both front surface and rear gap regions between contacts. To our knowledge, this is the first time that a c-Si solar cell with an IBC structure is fabricated entirely using ALD processes. Hence, this result opens the possibility to broaden the application of this deposition technique for cost-effective and high-volume manufacturing solar cells, increasing the ALD role in the future of photovoltaic industry [48,49].

The external-quantum-efficiency (EQE) of the best device is shown in Fig. 6 and its main photovoltaic parameters are summarised in Table 2. The excellent EQE values in the visible-NIR part of the spectrum, i.e. higher than 98% in the 500–1000 nm wavelength range, confirm an outstanding surface passivation, pointing out that carrier selective contacts based on ALD films are good enough to obtain high photovoltaic efficiencies. Open circuit voltage (V_{oc}) values above 700 mV are usual when an a-Si:H(i) passivation interlayer is used between the c-Si and the TMO [18,50,51]. Nonetheless, when the TMO is directly deposited on the c-Si surface, low V_{oc} values below 600 mV are typically

Table 2
Photovoltaic parameters for the best IBC solar cell using ALD V_2O_5 films (this work). Results are directly compared with an IBC counterpart where the V_2O_5 was deposited by thermal evaporation (data extracted from Ref. [20]). IBC solar cells have an active area of 3 cm × 3 cm and were measured under standard test conditions (1 kW/m^2 AM1.5G spectrum at 25 °C).

Parameter	Selective contact process (HTL – ETL) V_2O_5 – Al_2O_x/TiO_x	
	Evap. – ALD [20]	ALD – ALD [*this work*]
J_{sc} (mA/cm^2)	40.0	39.4
V_{oc} (mV)	633	652
FF (%)	75.4	72.5
p*FF* (%)	76.3	82.3
r_s (Ωcm^2)	0.19	1.97
η (%)	19.1	18.6
pseudo-η (%)	19.3	21.1

reported in the literature [9,26]. Consequently, the V_{oc} values of up to 652 mV achieved in this work can be considered a remarkable result. The other photovoltaic parameters listed in Table 2, such as the short circuit current density (J_{sc}), the fill factor (*FF*) and the power conversion efficiency (η), with values of 39.4 mA/cm^2, 72.5% and 18.6%, respectively, confirm the feasibility of ALD-based selective contacts for high efficiency IBC solar cells.

In order to get a better insight of the factors that may limit the performance of the device, we analysed the pseudo-light current density – voltage curve from Suns-V_{oc} measurements [52,53]. Fig. 8a shows the illuminated *J-V* curve for the best ALD V_2O_5-based IBC solar cell compared to the corresponding pseudo-light *J-V* curve. The difference between both curves suggests that there is a relevant power efficiency loss due to series resistance. This fact is corroborated by the high value (~2 Ωcm^2) of the specific series resistance (r_s) parameter, as well as by the significant difference between the *FF* and the pseudo fill factor (p*FF*) values. An estimation of the r_s parameter was calculated using the *FF* and p*FF* as follows; $r_s \cong (1 - FF/pFF)V_{oc}/J_{sc}$ [53].

The relatively high r_s parameter can be not only attributed to a higher contact resistivity of the ALD V_2O_5-based contact, in comparison with the thermally evaporated counterpart, but also for some problems during the metallisation stage, i.e. either insufficient Al thickness or a poor metallic pad coverage. However, the promising pseudo efficiency obtained with a value of 21.1% indicates that there is room for improvement in the future to increase the efficiency.

On the other hand, we can observe an important improvement in the pseudo-efficiency compared to the case of evaporated V_2O_x films mainly coming from the p*FF*, i.e. the ideality of the current mechanisms at the junction. Fig. 8b shows the dark *J-V* curves of two IBC solar cells, one based on ALD V_2O_5 films (this work) and another which uses thermally evaporated V_2O_x films for the hole-selective contact (see Ref. [20]). As discussed above, the ALD-based cell exhibits a higher series resistance that can be observed at high applied voltages. By contrast, it has a better dark *J-V* characteristic, i.e. a higher V_{oc} value than the evaporated counterpart, with an improvement of ~20 mV (see Table 2). In addition, there is a significant reduction in recombination losses at low injection, which could be due to a better V_2O_5 coverage at the edges of the HTL interdigitated regions provided by the ALD technique. The inset of Fig. 8b shows a cross section sketch explaining the potential coverage problem at the HTL edges when thermally evaporated V_2O_x films are used which can lead to non-ideal current mechanisms, i.e. low p*FF* values. This phenomenon was recently studied, see Ref. [31], pointing out the influence of the edge recombination in silicon-based IBC solar cells with dopant-free heterojunctions. Thus, the use of the ALD technique could be a good choice to circumvent this issue due to the conformal nature of this deposition technique.

4. Conclusions

In this work, we extensively report the characterisation of ALD V_2O_5 films to be applied as hole-selective contacts for IBC solar cells. ALD deposition parameters were studied to obtain a self-saturation regime with a V_2O_5 growth rate of ~0.6 Å/cycle. The X-ray photoelectron spectroscopy scan and its analysis for an ALD V_2O_5 film deposited at 125 °C, indicate that the film has a stoichiometric composition. The presence of an inverted layer in the c-Si(n) surface underneath the V_2O_5 film is confirmed by transfer length method (TLM) measurements, measuring sheet resistance (R_{sh}) values in the 11–16 kΩ/sq range.

The good contact passivation provided by ALD V_2O_5 films allowed recombination current densities (J_{0c}) between 80 and 150 fA/cm^2 for an ALD deposition temperature from 100 to 150 °C. In addition, the presence of a Ni metal capping did not degrade the contact passivation that even improved after a temperature treatment in N_2 ambient, i.e. a J_{0c} drop of 30% after 10 min annealing at 125 °C was measured.

Conduction properties of the ALD V_2O_5-based contact were studied by TLM measurements on c-Si(n) substrates. The ALD V_2O_5 films have a strong dependence with the film thickness and temperature process, obtaining a minimum contact resistivity (ρ_c) of 250 mΩcm^2 for 200 ALD cycles at 125 °C. For samples on c-Si(p) substrates, the ρ_c value is reduced to 100 mΩcm^2. After an annealing step at 125 °C, although the passivation quality improves, but the contact resistivity is strongly degraded. Therefore, the V_2O_5-based selective contact should be deposited at the last stages of the IBC fabrication process to prevent any degradation during high thermal steps.

Finally, the optimised ALD V_2O_5 film was applied to a proof-of-concept 3 × 3 cm^2 IBC c-Si(n) solar cell as a hole-selective contact. The TiO_2-based electron-selective contact is also deposited by ALD, as well as the Al_2O_3 films to passivate the non-contacted surfaces.

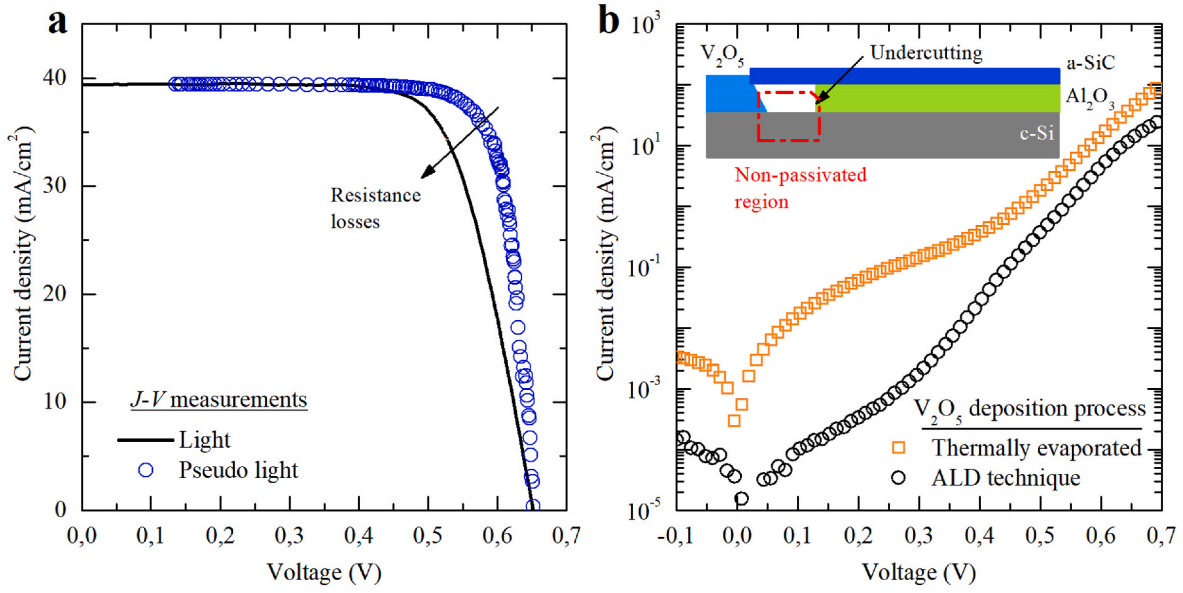

Fig. 8. (a) Light and pseudo light current density – voltage (*J–V*) curves for the best IBC solar cell. The pseudo *J-V* characteristic, free of series resistance effects, is determined from Suns-V_{oc} measurements. (b) Comparison of the dark *J-V* characteristic for the best IBC solar cell with a counterpart which uses thermal evaporated V_2O_5 films. In both cases, the ETL is based on TiO_2 films deposited by ALD. The inset shows a sketch of the undercutting phenomenon that could happen in the finger perimeter when thermal evaporation technique is used.

Consequently, to our knowledge, this is the first fully ALD IBC solar cell structure reported in the literature. A solar cell efficiency of 18.6% and a pseudo efficiency, i.e. calculated without losses due to parasitic series resistance, of 21.1% have been obtained. This work demonstrates the feasibility of applying the ALD technique to deposit carrier-selective contacts based on transition metal oxides for high efficiency IBC solar cells.

CRediT authorship contribution statement

Gerard Masmitjà: Writing – original draft, Methodology, Investigation, Formal analysis, Conceptualization. **Eloi Ros:** Investigation, Writing – review & editing. **Rosa Almache-Hernández:** Investigation, Formal analysis. **Benjamín Pusay:** Formal analysis, Investigation. **Isidro Martín:** Writing – review & editing, Methodology, Funding acquisition, Conceptualization. **Cristóbal Voz:** Conceptualization, Funding acquisition, Methodology, Writing – review & editing. **Edgardo Saucedo:** Funding acquisition, Conceptualization. **Joaquim Puigdollers:** Conceptualization, Funding acquisition, Methodology, Supervision, Writing – review & editing. **Pablo Ortega:** Writing – review & editing, Supervision, Methodology, Funding acquisition, Conceptualization.

Declaration of competing interest

The authors declare that they have no known competing financial interests or personal relationships that could have appeared to influence the work reported in this paper.

Acknowledgments

This work has been supported by the Spanish government under projects PID2019-109215RB-C41 (SCALED), PID2020-116719RB-C41 (MATER ONE) and PID2020-115719RB-C21 (GETPV) funded by MCIN/AEI/10.13039/501100011033. G. M. acknowledges financial support from the Grant UPC Margarita Salas 2021 of the Spanish Ministry of Universities and the European Unión (NextGenerationEU). R. A.-H. and B. P. acknowledge financial support from the International Grants SENESCYT-2018 of the Ecuadorian Government. The authors would like to thanks the Prof. Jordi Llorca for his help and discussion about XPS measurements carried out at the Barcelona Research Center in Multiscale Science and Engineering, and Dr Rodrigo Fernández-Pacheco of the Laboratorio de Microscopias Avanzadas (LMA-INA) of Zaragoza for the SEM images and EDX analysis.

References

[1] R. Singh, Why silicon is and will remain the dominant photovoltaic material, J. Nanophotonics 3 (2009), 032503, https://doi.org/10.1117/1.3196882.
[2] K. Yamamoto, K. Yoshikawa, H. Uzu, D. Adachi, High-efficiency heterojunction crystalline Si solar cells, in: Japanese Journal of Applied Physics, Japan Society of Applied Physics, 2018, https://doi.org/10.7567/JJAP.57.08RB20, 08RB20.
[3] M.D. Lammert, R.J. Schwartz, The interdigitated back contact solar cell: a silicon solar cell for use in concentrated sunlight, IEEE Trans. Electron. Dev. 24 (1977) 337–342, https://doi.org/10.1109/T-ED.1977.18738.
[4] Z.C. Holman, A. Descoeudres, L. Barraud, F.Z. Fernandez, J.P. Seif, S. De Wolf, C. Ballif, Current losses at the front of silicon heterojunction solar cells, IEEE Journal of Photovoltaics 2 (2012) 7–15, https://doi.org/10.1109/JPHOTOV.2011.2174967.
[5] E.L. Warren, W.E. Mcmahon, M. Rienäcker, K.T. Vansant, R.C. Whitehead, R. Peibst, A.C. Tamboli, A taxonomy for three-terminal tandem solar cells, ACS Energy Lett. 5 (2020) 1233–1242, https://doi.org/10.1021/acsenergylett.0c00068.
[6] M. Rienäcker, E.L. Warren, M. Schnabel, H. Schulte-Huxel, R. Niepelt, R. Brendel, P. Stradins, A.C. Tamboli, R. Peibst, Back-contacted bottom cells with three terminals: maximizing power extraction from current-mismatched tandem cells, Prog. Photovoltaics Res. Appl. 27 (2019) 410–423, https://doi.org/10.1002/pip.3107.
[7] F. Gota, M. Langenhorst, R. Schmager, J. Lehr, U.W. Paetzold, Energy yield advantages of three-terminal perovskite-silicon tandem photovoltaics, Joule 4 (2020) 2387–2403, https://doi.org/10.1016/J.JOULE.2020.08.021.
[8] M.T. Greiner, M.G. Helander, W.-M. Tang, Z.-B. Wang, J. Qiu, Z.-H. Lu, Universal energy-level alignment of molecules on metal oxides, Nat. Mater. 11 (2012) 76–81, https://doi.org/10.1038/nmat3159.
[9] L.G. Gerling, S. Mahato, A. Morales-Vilches, G. Masmitja, P. Ortega, C. Voz, R. Alcubilla, J. Puigdollers, Transition metal oxides as hole-selective contacts in silicon heterojunctions solar cells, Sol. Energy Mater. Sol. Cell. 145 (2016) 109–115, https://doi.org/10.1016/j.solmat.2015.08.028.
[10] J. Bullock, A. Cuevas, T. Allen, C. Battaglia, Molybdenum oxide MoO_x: a versatile hole contact for silicon solar cells, Appl. Phys. Lett. 105 (2014) 232109, https://doi.org/10.1063/1.4903467.
[11] K.A. Nagamatsu, S. Avasthi, G. Sahasrabudhe, G. Man, J. Jhaveri, A.H. Berg, J. Schwartz, A. Kahn, S. Wagner, J.C. Sturm, Titanium dioxide/silicon hole-blocking selective contact to enable double-heterojunction crystalline silicon-based solar cell, Appl. Phys. Lett. 106 (2015) 123906, https://doi.org/10.1063/1.4916540.
[12] Y. Wan, C. Samundsett, J. Bullock, M. Hettick, T. Allen, D. Yan, J. Peng, Y. Wu, J. Cui, A. Javey, A. Cuevas, Conductive and stable magnesium oxide electron-selective contacts for efficient silicon solar cells, Adv. Energy Mater. 7 (2017) 1601863, https://doi.org/10.1002/aenm.201601863.
[13] J. Bullock, M. Hettick, J. Geissbühler, A.J. Ong, T. Allen, C.M. Sutter-Fella, T. Chen, H. Ota, E.W. Schaler, S. De Wolf, C. Ballif, A. Cuevas, A. Javey, Efficient silicon solar cells with dopant-free asymmetric heterocontacts, Nat. Energy 1 (2016) 15031, https://doi.org/10.1038/nenergy.2015.31.
[14] Z. Yang, J. Yan, W. Yang, Y. Zeng, J. Sun, X. Wang, X. Yang, J.C. Greer, J. Sheng, B. Yan, J. Ye, Back-contact structures for optoelectronic devices: applications and perspectives, Nano Energy 78 (2020), https://doi.org/10.1016/j.nanoen.2020.105362.
[15] T.G. Allen, J. Bullock, X. Yang, A. Javey, S. de Wolf, Passivating contacts for crystalline silicon solar cells, Nature Energy 2019 4:11 4 (2019) 914–928, https://doi.org/10.1038/S41560-019-0463-6.
[16] J. Melskens, B.W.H. van de Loo, B. Macco, L.E. Black, S. Smit, W.M.M. Kessels, Passivating contacts for crystalline silicon solar cells: from concepts and materials to prospects, IEEE Journal of Photovoltaics 8 (2018) 373–388, https://doi.org/10.1109/JPHOTOV.2018.2797106.
[17] G. Gregory, C. Luderer, H. Ali, T.S. Sakthivel, T. Jurca, M. Bivour, S. Seal, K. O. Davis, Spatial atomic layer deposition of molybdenum oxide for industrial solar cells, Adv. Mater. Interfac. 7 (2020), https://doi.org/10.1002/admi.202000895, 2000895.
[18] X. Yang, H. Xu, W. Liu, Q. Bi, L. Xu, J. Kang, M.N. Hedhili, B. Sun, X. Zhang, S. De Wolf, Atomic layer deposition of vanadium oxide as hole-selective contact for crystalline silicon solar cells, Advanced Electronic Materials 6 (2020) 2000467, https://doi.org/10.1002/aelm.202000467.
[19] B. Macco, L.E. Black, J. Melskens, B.W.H. van de Loo, W.J.H. Berghuis, M. A. Verheijen, W.M.M. Kessels, Atomic-layer deposited Nb2O5 as transparent passivating electron contact for c-Si solar cells, Sol. Energy Mater. Sol. Cell. 184 (2018) 98–104, https://doi.org/10.1016/J.SOLMAT.2018.04.037.
[20] G. Masmitjà, P. Ortega, J. Puigdollers, L.G. Gerling, I. Martín, C. Voz, R. Alcubilla, Interdigitated back-contacted crystalline silicon solar cells with low-temperature dopant-free selective contacts, J. Mater. Chem. 6 (2018) 3977–3985, https://doi.org/10.1039/C7TA11308K.
[21] G. Chistiakova, B. MacCo, L. Korte, Low-temperature atomic layer deposited magnesium oxide as a passivating electron contact for c-Si-based solar cells, IEEE Journal of Photovoltaics 10 (2020) 398–406, https://doi.org/10.1109/JPHOTOV.2019.2961603.
[22] P. Poodt, D.C. Cameron, E. Dickey, S.M. George, V. Kuznetsov, G.N. Parsons, F. Roozeboom, G. Sundaram, A. Vermeer, Spatial atomic layer deposition: a route towards further industrialization of atomic layer deposition, J. Vac. Sci. Technol.: Vacuum, Surfaces, and Films 30 (2012), 010802, https://doi.org/10.1116/1.3670745.
[23] P. Poodt, A. Lankhorst, F. Roozeboom, K. Spee, D. Maas, A. Vermeer, High-speed spatial atomic-layer deposition of aluminum oxide layers for solar cell passivation, Adv. Mater. 22 (2010) 3564–3567, https://doi.org/10.1002/adma.201000766.
[24] E.R. Costals, G. Masmitjà, E. Almache, B. Pusay, K. Tiwari, E. Saucedo, C.J. Raj, B. C. Kim, J. Puigdollers, I. Martin, C. Voz, P. Ortega, Atomic layer deposition of vanadium oxide films for crystalline silicon solar cells, Materials Advances (2021), https://doi.org/10.1039/D1MA00812A.
[25] H.-D. Um, N. Kim, K. Lee, I. Hwang, J.H. Seo, K. Seo, Dopant-free all-back-contact Si nanohole solar cells using MoOx and LiF films, Nano Lett. 16 (2016) 981–987, https://doi.org/10.1021/acs.nanolett.5b03955.
[26] W. Wu, J. Bao, X. Jia, Z. Liu, L. Cai, B. Liu, J. Song, H. Shen, Dopant-free back contact silicon heterojunction solar cells employing transition metal oxide emitters, Phys. Status Solidi Rapid Res. Lett. 10 (2016) 662–667, https://doi.org/10.1002/pssr.201600254.
[27] W. Wu, W. Lin, J. Bao, Z. Liu, B. Liu, K. Qiu, Y. Chen, H. Shen, Dopant-free multilayer back contact silicon solar cells employing V2Ox/metal/V2Ox as an emitter, RSC Adv. 7 (2017) 23851–23858, https://doi.org/10.1039/c7ra03368k.
[28] W. Wu, W. Lin, S. Zhong, B. Paviet-Salomon, M. Despeisse, Z. Liang, M. Boccard, H. Shen, C. Ballif, 22% efficient dopant-free interdigitated back contact silicon solar cells, in: AIP Conference Proceedings, AIP Publishing LLC, 2018, https://doi.org/10.1063/1.5049288, 040025.
[29] H. Lin, D. Ding, Z. Wang, L. Zhang, F. Wu, J. Yu, P. Gao, J. Ye, W. Shen, Realization of interdigitated back contact silicon solar cells by using dopant-free heterocontacts for both polarities, Nano Energy 50 (2018) 777–784, https://doi.org/10.1016/J.NANOEN.2018.06.013.
[30] F. Li, Z. Sun, Y. Zhou, Q. Wang, Q. Zhang, G. Dong, F. Liu, Z. Fan, Z. Liu, Z. Cai, Y. Zhou, D. Yu, Lithography-free and dopant-free back-contact silicon

heterojunction solar cells with solution-processed TiO2 as the efficient electron selective layer, Sol. Energy Mater. Sol. Cell. 203 (2019) 110196, https://doi.org/10.1016/J.SOLMAT.2019.110196.
[31] H. Lin, J. Wang, Z. Wang, Z. Xu, P. Gao, W. Shen, Edge effect in silicon solar cells with dopant-free interdigitated back-contacts, Nano Energy 74 (2020) 104893, https://doi.org/10.1016/J.NANOEN.2020.104893.
[32] W. Wu, W. Lin, S. Zhong, B. Paviet-Salomon, M. Despeisse, Q. Jeangros, Z. Liang, M. Boccard, H. Shen, C. Ballif, Dopant-free back-contacted silicon solar cells with an efficiency of 22.1, Phys. Status Solidi Rapid Res. Lett. 14 (2020) 1900688, https://doi.org/10.1002/PSSR.201900688.
[33] G. Masmitjà, L.G. Gerling, P. Ortega, J. Puigdollers, I. Martín, C. Voz, R. Alcubilla, V2Ox-based hole-selective contacts for c-Si interdigitated back-contacted solar cells, J. Mater. Chem. 5 (2017) 9182–9189, https://doi.org/10.1039/C7TA01959A.
[34] W. Kern, The evolution of silicon wafer cleaning technology, J. Electrochem. Soc. 137 (1990) 1887, https://doi.org/10.1149/1.2086825.
[35] B. Hoex, J. Schmidt, P. Pohl, M.C.M. van de Sanden, W.M.M. Kessels, Silicon surface passivation by atomic layer deposited Al2O3, J. Appl. Phys. 104 (2008), 044903, https://doi.org/10.1063/1.2963707.
[36] R.A. Sinton, A. Cuevas, M. Stuckings, Quasi-steady-state photoconductance, a new method for solar cell material and device characterization, in: Conference Record of the Twenty Fifth IEEE Photovoltaic Specialists Conference - 1996, IEEE, 1996, pp. 457–460, https://doi.org/10.1109/PVSC.1996.564042.
[37] H.H. Berger, Contact resistance and contact resistivity, J. Electrochem. Soc. 119 (1972) 507–514, https://doi.org/10.1149/1.2404240.
[38] S. Guo, G. Gregory, A.M. Gabor, W.V. Schoenfeld, K.O. Davis, Detailed investigation of TLM contact resistance measurements on crystalline silicon solar cells, Sol. Energy 151 (2017) 163–172, https://doi.org/10.1016/j.solener.2017.05.015.
[39] R.H. Cox, H. Strack, Ohmic contacts for GaAs devices, Solid State Electron. 10 (1967) 1213–1218, https://doi.org/10.1016/0038-1101(67)90063-9.
[40] J. Musschoot, D. Deduytsche, H. Poelman, J. Haemers, R.L. Van Meirhaeghe, S. Van den Berghe, C. Detavernier, Comparison of thermal and plasma-enhanced ALD/CVD of vanadium pentoxide, J. Electrochem. Soc. 156 (2009) P122, https://doi.org/10.1149/1.3133169.
[41] G.Y. Song, C. Oh, S. Sinha, J. Son, J. Heo, Facile phase control of multivalent vanadium oxide thin films (V2O5 and VO2) by atomic layer deposition and postdeposition annealing, ACS Appl. Mater. Interfaces 9 (2017) 23909–23917, https://doi.org/10.1021/acsami.7b03398.
[42] B.E. Davis, N.C. Strandwitz, Aluminum oxide passivating tunneling interlayers for molybdenum oxide hole-selective contacts, IEEE Journal of Photovoltaics 10 (2020) 722–728, https://doi.org/10.1109/JPHOTOV.2020.2973447.
[43] M.T. Greiner, L. Chai, M.G. Helander, W.M. Tang, Z.H. Lu, Metal/metal-oxide interfaces: how metal contacts affect the work function and band structure of MoO3, Adv. Funct. Mater. 23 (2013) 215–226, https://doi.org/10.1002/adfm.201200993.
[44] A. Richter, S.W. Glunz, F. Werner, J. Schmidt, A. Cuevas, Improved quantitative description of Auger recombination in crystalline silicon, Phys. Rev. B 86 (2012) 165202, https://doi.org/10.1103/PhysRevB.86.165202.
[45] A. Cuevas, D. Macdonald, Measuring and interpreting the lifetime of silicon wafers, Sol. Energy 76 (2004) 255–262, https://doi.org/10.1016/j.solener.2003.07.033.
[46] K. Zilberberg, S. Trost, J. Meyer, A. Kahn, A. Behrendt, D. Lützenkirchen-Hecht, R. Frahm, T. Riedl, Inverted organic solar cells with sol-gel processed high work-function vanadium oxide hole-extraction layers, Adv. Funct. Mater. 21 (2011) 4776–4783, https://doi.org/10.1002/adfm.201101402.
[47] L.G. Gerling, C. Voz, R. Alcubilla, J. Puigdollers, Origin of passivation in hole-selective transition metal oxides for crystalline silicon heterojunction solar cells, J. Mater. Res. 32 (2017) 260–268, https://doi.org/10.1557/jmr.2016.453.
[48] J.A. Van Delft, D. Garcia-Alonso, W.M.M. Kessels, Atomic layer deposition for photovoltaics: applications and prospects for solar cell manufacturing, Semicond. Sci. Technol. 27 (2012), 074002, https://doi.org/10.1088/0268-1242/27/7/074002.
[49] MdA. Hossain, K.T. Khoo, X. Cui, G.K. Poduval, T. Zhang, X. Li, W.M. Li, B. Hoex, Atomic layer deposition enabling higher efficiency solar cells: a review, Nano Materials Science 2 (2020) 204–226, https://doi.org/10.1016/j.nanoms.2019.10.001.
[50] M. Bivour, J. Temmler, H. Steinkemper, M. Hermle, Molybdenum and tungsten oxide: high work function wide band gap contact materials for hole selective contacts of silicon solar cells, Sol. Energy Mater. Sol. Cell. 142 (2015) 34–41, https://doi.org/10.1016/j.solmat.2015.05.031.
[51] J. Geissbühler, J. Werner, S. Martin de Nicolas, L. Barraud, A. Hessler-Wyser, M. Despeisse, S. Nicolay, A. Tomasi, B. Niesen, S. De Wolf, C. Ballif, 22.5% efficient silicon heterojunction solar cell with molybdenum oxide hole collector, Appl. Phys. Lett. 107 (2015), 081601, https://doi.org/10.1063/1.4928747.
[52] R.A. Sinton, A. Cuevas, A quasi-steady-state open-circuit voltage method for solar cell characterization, in: Proceedings of the 16th European Photovoltaic Solar Energy Conference, 2000, pp. 1–5. Glasgow.
[53] P.R. Ortega, J.M. Pinol, I. Martin, A. Orpella, G. Masmitja, G. Lopez, E. Ros, C. Voz, J. Puigdollers, R. Alcubilla, Low-cost high-sensitive suns-voc measurement instrument to characterize c-Si solar cells, IEEE Trans. Instrum. Meas. 69 (2020) 6429–6435, https://doi.org/10.1109/TIM.2020.2967136.